This article has been accepted for publication in a future issue of this journal, but has not been fully edited. Content may change prior to final publication. Citation information: DOI 10.1109/TIE.2014.2327562, IEEE Transactions on Industrial Electronics

Balancing and Velocity Control of a Unicycle Robot Based on the Dynamic Model

Seong I. Han, *Member, IEEE*, and Jang M. Lee, *Senior Member, IEEE*

***Abstract*—This paper presents a dynamic model-based control scheme for the balancing and velocity control of a unicycle robot. Unicycle robot motion consists of a pitch that is controlled by an in-wheel motor and a roll that is controlled by a reaction wheel pendulum. The unicycle robot lacks an actuator for yaw-axis control, which makes the derivation of the dynamics relatively simple even though it may limit the motion control. The Euler–Lagrange equation is applied to derive the dynamic equations of the unicycle robot to implement dynamic speed control. To achieve real-time speed control, a sliding mode control and a nonzero set-point LQ regulator (LQR) are utilized to guarantee stability while maintaining the desired speed-tracking performance. In the roll controller, a sigmoid-function-based sliding mode controller has been adopted to minimize switching-function chattering. An LQR controller has been implemented for pitch control to drive the unicycle robot to follow the desired velocity trajectory in real time using the state variables of pitch angle, angular velocity, wheel angle, and angular velocity. The control performance of the two control systems using a single dynamic model has been experimentally demonstrated.**

***Index Terms*— Unicycle robot, dynamic equation, velocity and trajectory control, nonzero set-point LQR, sliding mode control**

I. INTRODUCTION

Research on the single-wheel (unicycle) robot has been under way since the 1980s in the United States and Japan [1], [2]. A. Schoonwinkel of Stanford university proposed a linear dynamic model for the robot and presented its optimal motion control [3], [4]. A professor of Tokyo University also proposed a dynamic model for the robot that comprised an upper turntable and a lower rotating wheel [5]. Honda developed UX-3 as a personal mobility system, and Murata Manufacturing also developed Murata Girl on a single wheel. Most of the research on the single-wheel robot has focused on the stable driving of the single wheel without considering a specific types of trajectory control. Currently, there is a study that implements trajectory control assuming that the dynamics of the upper reaction wheel pendulum and lower inverted pendulum are decoupled [6]. In the study, the coupling terms are compensated by an intelligent algorithm such as fuzzy interferences. For the high-speed motion of the single-wheel robot, the coupling terms become large and time varying. Therefore, the intelligent algorithm is not adequate for various trajectory controls [7-9]. As the applications of a unicycle robot, Murata manufacturing company exhibited a robot riding unicycle named "Murata Girl" in September 2008 [10]. Human riding unicycle model [11] and similar types of unicycle robot have been developed [12-14]. Air blowing and magnetic force balanced unicycle models are studied instead of disc rotation for side balancing of unicycle robot [15], [16].

In this paper, a new unicycle robot is designed and implemented. After deriving the dynamic equations of the unicycle robot, which is expressed as a three-dimensional (3D) model structure, a model-based controller is designed to maintain balance and to drive the unicycle robot to a desired location. Since the dynamic characteristics of the roll and pitch axes are different, two different controllers are designed for the balance of the roll axis and for the speed control of the pitch axis. First, the sliding mode control is applied to the roll axis [17-21]. When a controlled variable of the sliding mode control meets the Lyapunov stability condition, the controller can stably maintain the control states. In designing the sliding mode controller, the key issue is to find appropriate controlled variables. The chattering problem of the sliding mode control, which used the signum function as a switching function, is also resolved in this study. The chattering phenomenon damages actuators and disturbs the system states. Thus, the chattering must be attenuated to an acceptable level. In this study, first, the chattering is greatly reduced by using a sigmoidal function such as the tanh function. Second, the nonzero set-point LQ regulator [22], [23] is designed with the weighting matrices for pitch-axis control. With this LQR controller, the balance and speed controls are operated concurrently.

After this introduction, system modeling is expressed in Section II. In Section III, the design of control system is illustrated in detail. Results of experiments are demonstrated in Section IV, and finally in Section V, the conclusions and future research works are summarized and suggested.

Manuscript received December 8, 2013; revised March 20, 2014; accepted May 10, 2014.

This work was supported by the National Research Foundation of Korea (NRF) Grant funded by the Korean Government (MSIP). (NRF-2013R1A1A 2021174)

S. I. Han is with the Department of Electronic Engineering, Pusan National University, Busan, 609-735 Republic of Korea (e-mail:skhan@pusan.ac.kr).

J. M. Lee is with the Department of Electronic Engineering, Pusan National University, Busan, 609-735 Republic of Korea (phone: 82-51-510-2378; fax:82-51-514-1693; e-mail:jmlee@pusan.ac.kr).

This article has been accepted for publication in a future issue of this journal, but has not been fully edited. Content may change prior to final publication. Citation information: DOI 10.1109/TIE.2014.2327562, IEEE Transactions on Industrial Electronics

II. SYSTEM MODELING

In this section, the dynamic equations of the unicycle robot

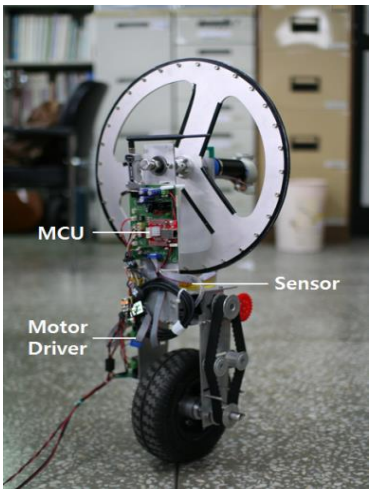

Fig. 1. Unicycle robot.

are derived. In Fig.1, the disc is installed on the top to generate a rotational inertia and the central axis of the disc is maintained as the center of gravity. Therefore, the upper part of the unicycle is a reaction wheel pendulum and the lower part can be modeled as an inverted pendulum.

There are a few methods that can be used to obtain the dynamic equations of a system. In this paper, the Lagrange equation is used to derive the dynamic equations, which can be used for the design of the simulation and control systems.

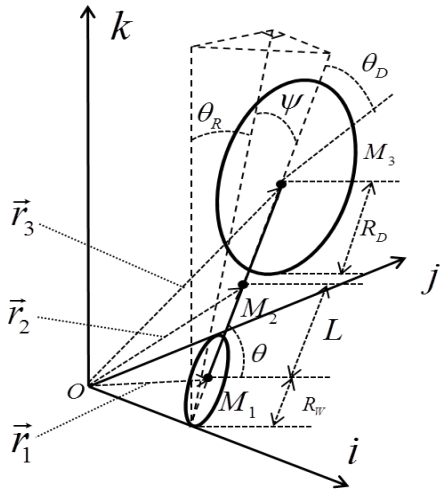

Fig. 2. Structure map of the unicycle robot.

A structure map of the unicycle robot is defined and drawn in 3D space to reveal the physical characteristics of the unicycle robot for the dynamic model. The reference axis is set as $\{i, j, k\}$ in Fig. 2, where L represents the length from the center of the wheel to the center of the body. R_D and R_w denote the radius of the disc and the wheel, respectively. θ_R represents the angle of the roll axis, and θ defines the angle of the wheel. ψ and θ_D denote the angles of the pitch axis and the disc, respectively. M_1, M_2, and M_3 denote the masses of the wheel, body, and disc, respectively [24].

Generally, to obtain the dynamic equations from the Lagrange equation, the kinetic and potential energy terms are required. Kinetic energy consists of translational and rotational kinetic energies. First, position vectors are defined to obtain the translational kinetic energy. In Fig. 2, $\vec{r}_1$, $\vec{r}_2$, and $\vec{r}_3$ represent the position vectors of the wheel, body, and disc, respectively, and are defined as follows:

$$\vec{r}_1 = R_w\theta\hat{i} + R_w s\theta_R\hat{j} + R_w c\theta_R\hat{k}\,, \tag{1}$$

$$\vec{r}_2 = (R_w\theta + Ls\psi)\hat{i} + (R_w s\theta_R + Lc\psi s\theta_R)\hat{j} + (R_w c\theta_R + Lc\psi c\theta_R)\hat{k}\,, \tag{2}$$

$$\vec{r}_3 = (R_w\theta + 2Ls\psi)\hat{i} + (R_w s\theta_R + 2Lc\psi s\theta_R)\hat{j} + (R_w c\theta_R + 2Lc\psi c\theta_R)\hat{k}\,, \tag{3}$$

where $s(\cdot)$ and $c(\cdot)$ mean $\sin(\cdot)$ and $\cos(\cdot)$, respectively. From the position vectors, the velocity vectors are obtained as follows:

$$\vec{v}_1 = R_w\dot{\theta}\hat{i} + R_w\dot{\theta}_R c\theta_R\hat{j} - R_w\dot{\theta}_R s\theta_R\hat{k}\,, \tag{4}$$

$$\vec{v}_2 = (L\dot{\psi}c\psi + R_w\dot{\theta})\hat{i} + (-L\dot{\psi}s\psi s\theta_R + R_w\dot{\theta}_R c\theta_R + L\dot{\theta}_R c\psi c\theta_R)\hat{j} + (-L\dot{\psi}c\theta_R s\psi - R_w\dot{\theta}_R s\theta_R - L\dot{\theta}_R s\psi s\theta_R)\hat{k}\,, \tag{5}$$

$$\vec{v}_3 = (2L\dot{\psi}c\psi + R_w\dot{\theta})\hat{i} + (-2L\dot{\psi}s\psi s\theta_R + R_w\dot{\theta}_R c\theta_R + 2L\dot{\theta}_R c\psi c\theta_R)\hat{j} + (-2L\dot{\psi}c\theta_R s\psi - R_w\dot{\theta}_R s\theta_R - 2L\dot{\theta}_R c\psi s\theta_R)\hat{k}\,. \tag{6}$$

The total kinetic energy T is obtained as the sum of translational kinetic energy T_1 and rotational kinetic energy T_2:

$$T = T_1 + T_2\,, \tag{7}$$

$$T_1 = \frac{1}{2}M_1(\vec{v}_1\cdot\vec{v}_1) + \frac{1}{2}M_2(\vec{v}_2\cdot\vec{v}_2) + \frac{1}{2}M_3(\vec{v}_3\cdot\vec{v}_3)\,, \tag{8}$$

$$T_2 = \frac{1}{2}J_w\dot{\theta}^2 + \frac{1}{2}J_m n^2(\dot{\theta}-\dot{\psi})^2 + \frac{1}{2}J_\psi\dot{\psi}^2 + \frac{1}{2}J_d(\dot{\theta}_R + \dot{\theta}_D)^2\,. \tag{9}$$

From Fig. 2, the potential energy of the unicycle robot is obtained as

$$U = M_1 g R_w c\theta_R + M_2 g(R_w c\theta_R + Lc\psi c\theta_R) + M_3 g(R_w c\theta_R + 2Lc\psi c\theta_R)\,. \tag{10}$$

The Lagrangian, the difference between the kinetic energy and potential energies, is given by

$$L = T - U. \tag{11}$$

Substituting L into the Lagrange dynamic equation, the dynamic equations of the unicycle robot are obtained as follows:

$$\frac{d}{dt}\left(\frac{\partial L}{\partial\dot{q}}\right) - \frac{\partial L}{\partial q} = \tau_q\,, \tag{12}$$

This article has been accepted for publication in a future issue of this journal, but has not been fully edited. Content may change prior to final publication. Citation information: DOI 10.1109/TIE.2014.2327562, IEEE Transactions on Industrial Electronics

where $q=\begin{bmatrix}\theta_R & \theta_D & \psi & \theta\end{bmatrix}^T$. From Eq. (9), the dynamic equations of the system states of the unicycle robot are obtained as follows:

$$M(q)\ddot{q}+C(q,\dot{q})\dot{q}+G(q)=\tau_q, \tag{13}$$

where

$$M(q)=\begin{bmatrix}M_{11} & M_{12} & M_{13} & 0\\ M_{21} & M_{22} & 0 & 0\\ M_{31} & 0 & M_{33} & M_{34}\\ 0 & 0 & M_{43} & M_{44}\end{bmatrix},$$

$$C(q,\dot{q})=\begin{bmatrix}C_{11} & 0 & C_{13} & 0\\ 0 & 0 & 0 & 0\\ C_{31} & 0 & C_{33} & 0\\ 0 & 0 & C_{43} & 0\end{bmatrix},$$

$$G(q)=\begin{bmatrix}G_1 & 0 & G_3 & 0\end{bmatrix}^T,$$

$$\tau=\begin{bmatrix}\tau_R & \tau_D & \tau_\psi & \tau_\theta\end{bmatrix}^T,$$

$$\begin{aligned}M_{11}=\;& M_1R_w^2+M_2\left(R_w^2+L^2c^2\psi c^2\theta_R+2LR_wc^2\theta_Rc\psi\right.\\ &\left.+L^2s^2\psi s^2\theta_R+2LR_ws^2\theta_Rs\psi\right)\\ &+M_3\left(R_w^2+4L^2c^2\psi+4LR_wc\psi\right)+J_d,\end{aligned}$$

$$M_{12}=M_{21}=J_d,$$

$$M_{13}=M_{31}=M_2L^2s\theta_Rc\theta_R\left(-s\psi c\psi+s^2\psi\right),$$

$$M_{22}=J_d,$$

$$M_{33}=M_2L^2c^2\psi+M_34L^2c^2\psi-J_mn^2+J_\psi,$$

$$M_{34}=M_{43}=M_2LR_wc\psi+2M_3LR_wc\psi+J_mn^2,$$

$$M_{44}=M_2R_w^2+M_3R_w^2+J_w+J_mn^2,$$

$$\begin{aligned}C_{11}=\;& M_2(-L^2c^2\psi c\theta_Rs\theta_R-2LR_wc\theta_Rs\theta_Rc\psi\\ &+L^2s^2\psi s\theta_Rc\theta_R)\dot{\theta}_R+\left[M_2\left(-L^2c\psi s\psi c^2\theta_R\right.\right.\\ &\left.+L^2s^2\psi s\theta_Rc\theta_R+LR_ws^2\theta_Rc\psi\right)\\ &\left.+M_3\left(-4L^2c\psi s\psi-2LR_ws\psi\right)\right]\dot{\psi},\end{aligned}$$

$$\begin{aligned}C_{13}=\;& \left[M_2\left(-L^2c\psi s\psi c^2\theta_R-LR_wc^2\theta_Rs\psi\right.\right.\\ &\left.+L^2s\psi c\psi s^2\theta_R+LR_ws^2\theta_Rc\psi\right)\\ &\left.+M_3\left(-4L^2c\psi s\psi-2LR_ws\psi\right)\right]\dot{\theta}_R\\ &+M_2L^2(c^2\theta_R-s^2\theta_R)\left(-s\psi c\psi+s^2\psi\right)\dot{\psi},\end{aligned}$$

$$\begin{aligned}C_{31}=\;& \left[M_2L^2(c^2\theta_R-s^2\theta_R)\left(-s\psi c\psi+s^2\psi\right)\right.\\ &-M_2\left(-L^2c\psi s\psi c^2\theta_R-LR_wc^2\theta_Rs\psi\right.\\ &\left.\left.+L^2s\psi c\psi s^2\theta_R+LR_ws^2\theta_Rc\psi\right)\right]\dot{\theta}_R\end{aligned}$$

$$C_{33}=(-M_2L^2c\psi s\psi-4M_3L^2c\psi s\psi)\dot{\psi},$$

$$C_{43}=(-M_2LR_ws\psi-2M_3LR_ws\psi)\dot{\psi},$$

τ_R,τ_D,τ_ψ, and τ_θ represent the torques on the roll axis, disc, pitch axis, and wheel, respectively. According to the law of conservation of angular momentum, there are two constraint equations in each set of two torques: $\tau_R=-\tau_D$ and $\tau_\psi=-\tau_\theta$.

Since the motor drives are controlled by pulse width modulation, the torque inputs are required to be transformed to voltage inputs. The dynamic equations that express the torque inputs can be transformed to express voltage inputs by using the dynamic equations of DC motors. The torque of roll DC motor can be represented by the voltage as follows:

$$\tau_\theta=\frac{nk_t}{R_m}V-\left(\frac{nk_t}{R_m}k_b+f_m\right)(\dot{\theta}-\dot{\psi}), \tag{14}$$

$$\tau_D=\frac{nk_t}{R_m}V-\left(\frac{nk_t}{R_m}k_b+f_m\right)(\dot{\theta}_D-\dot{\theta}_R), \tag{15}$$

where V is the input voltage of the roll axis motor, n is motor gear ratio, R_m is the resistor coefficient of motor, k_t denotes the torque constant, f_m denotes the friction coefficient of the motor, and k_b denotes the back *emf* constant. Notice that the same motors and gears are used for the roll and pitch controllers. Therefore, the torque of the pitch and roll motor can be obtained directly as $\tau_\psi=-\tau_\theta$ and $\tau_R=-\tau_D$, respectively. For the simplicity, $\frac{nk_t}{R_m}$ and $\frac{nk_t}{R_m}k_b+f_m$ are renamed as α and β, respectively. In the design process of the controller for each axis, α and β are determined differently for each controller. Table I indicates the parameter values used in the dynamic equations.

TABLE I
UNICYLCE ROBOT PARAMETERS

Symbol	Parameter	Quantity
M_1, M_2, M_3	mass of wheel, body and disc	1.43kg, 4.08kg, 1.30kg
R_w, R_D	radius of wheel and disc	0.11m, 0.20m
L	length from the center of the wheel to the center of body	0.225m
g	gravity acceleration	9,806m/s^2
J_d	inertia of the disc	0.1840kgm^2
J_ψ	inertia of the robot body and the rotational disc	0.1951kgm^2
J_w	inertia of the wheel	0.0086kgm^2
J_m	inertia of the motor armature	0.0001kgm^2
J_b	inertia of the robot body and the wheel	0.0928kgm^2

III. CONTROLLER DESIGN

In this section, the controllers are designed based on the dynamic equations of the robot obtained in the previous section. The unicycle robot has two actuators that are separately located on the roll and pitch axes, and the controller design for these actuators is the major goal in

This article has been accepted for publication in a future issue of this journal, but has not been fully edited. Content may change prior to final publication. Citation information: DOI 10.1109/TIE.2014.2327562, IEEE Transactions on Industrial Electronics

this section. From previous experience with controlling this unicycle robot, the sliding mode controller and the nonzero set-point LQR controller are selected for the roll and pitch axes, respectively. Fig. 3 depicts the overall system block diagram of the unicycle robot. The states of the unicycle robot are defined as $\boldsymbol{q} = [\theta_R \;\; \dot{\theta}_R \;\; \theta_D \;\; \dot{\theta}_D \;\; \psi \;\; \dot{\psi} \;\; \theta \;\; \dot{\theta}]^T$. The system controllers of the sliding mode control for roll and the LQR control for pitch are placed in front of the system. The outputs of the controllers enter the system to control the actuators. Different references are specified for each axis of roll and pitch. The balance control is only implemented at the roll axis, while both the balance and driving controls are conducted at the pitch axis.

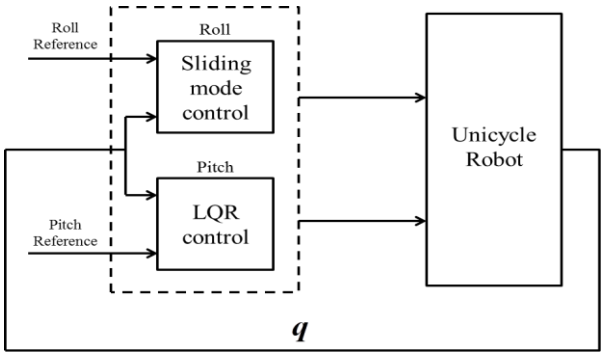

Fig. 3. Block diagram of the overall system.

A. Pitch controller

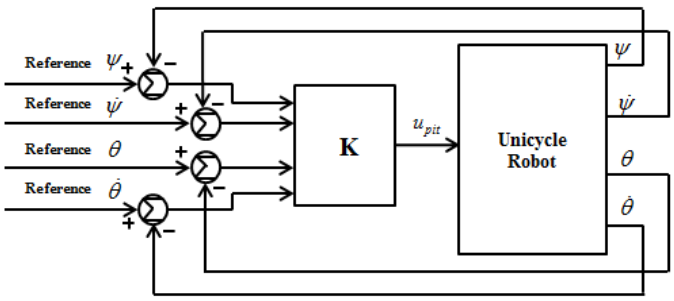

Fig. 4. Block diagram of the LQR control for the pitch controller.

Fig. 4 shows the control block diagram of the designed nonzero set-point LQR controller for controlling the pitch axis. K is defined as $[K_1, K_2, K_3, K_4]$ for each of four inputs. There are two references to control balance and driving simultaneously. Reference ψ is used for balance control, and reference θ is used for driving control.

To apply this state feedback optimal control, first, a system matrix and weight matrices need to be determined as follows:

$$\dot{x}_p = A_p x_p + B_p u_p , \tag{16}$$

where the system states are defined as $x_p = [\psi \;\; \dot{\psi} \;\; \theta \;\; \dot{\theta}]^T$, u_p represents input voltages, which are obtained from the dynamic equations expressed in terms of the voltage inputs. These equations can be derived by transforming torques to voltages by using DC motor dynamic equations.

The simplified pitch dynamics can be represented as follows:

$$\begin{aligned}\ddot{\psi} = \Big[& (M_2R_w^2 + M_3R_w^2 + J_w + J_m n^2)(-M_2L^2\psi - 4M_3L^2\psi)\dot{\psi}^2 \\ & -(M_2LR_w + 2M_3LR_w + J_m n^2)(-M_2R_wL\psi \\ & -2M_3LR_w\psi)\dot{\psi}^2 + (M_2R_w^2 + M_3R_w^2 + J_w \\ & + J_m n^2)(M_2gL + 2M_3gL)\psi + (-M_2R_w^2 - M_3R_w^2 - J_w \\ & -M_2LR_w - 2M_3LR_w - 2J_m n^2)(\alpha V - \beta(\dot{\theta} - \dot{\psi}))\Big] / \Big[(M_2R_w^2 \\ & + M_3R_w^2 + J_w + J_m n^2)(M_2L^2 + M_3 4L^2 - J_m n^2 + J_\psi) \\ & -(M_2LR_w + 2M_3LR_w + J_m n^2)^2 \Big], \end{aligned} \tag{17}$$

$$\begin{aligned}\ddot{\theta} = \Big[& -(M_2LR_w + 2M_3LR_w + J_m n^2)(-M_2L^2\psi - 4M_3L^2\psi)\dot{\psi}^2 \\ & +(M_2L^2 + M_3 4L^2 - J_m n^2 + J_\psi)(-M_2LR_w\psi \\ & -2M_3LR_w\psi)\dot{\psi}^2 - (M_2LR_w + 2M_3LR_w + \\ & + J_m n^2)(M_2gL + 2M_3gL)\psi + (M_2LR_w + 2M_3LR_w \\ & + M_2L^2 + 4M_3L^2 + J_\psi)(\alpha V + \beta(\dot{\theta} - \dot{\psi}))\Big] / \Big[(M_2R_w^2 \\ & + M_3R_w^2 + J_w + J_m n^2)(M_2L^2 + M_3 4L^2 - J_m n^2 + J_\psi) \\ & -(M_2LR_w + 2M_3LR_w + J_m n^2)^2 \Big]. \end{aligned} \tag{18}$$

(17) and (18) can be arranged to obtain the A and B matrices in (19). The resulting system matrix is represented as follows:

$$\begin{bmatrix} \dot{\psi} \\ \ddot{\psi} \\ \dot{\theta} \\ \ddot{\theta} \end{bmatrix} = \begin{bmatrix} 0 & 1 & 0 & 0 \\ A_{21} & A_{22} & 0 & A_{24} \\ 0 & 0 & 0 & 1 \\ A_{41} & A_{42} & 0 & A_{44} \end{bmatrix} \begin{bmatrix} \psi \\ \dot{\psi} \\ \theta \\ \dot{\theta} \end{bmatrix} + \begin{bmatrix} 0 \\ B_{21} \\ 0 \\ B_{41} \end{bmatrix} u_{pit} , \tag{19}$$

where

$$\begin{aligned} A_{21} &= (M_2R_w^2 + M_3R_w^2 + J_w + J_m n^2)(M_2 + 2M_3)gL / D_{pit} , \\ A_{22} &= (M_2R_w^2 + M_3R_w^2 + J_w + J_m n^2)(-M_2L^2\psi \\ &\quad -4M_3L^2\psi)\dot{\psi} - (M_2R_wL + 2M_3LR_w \\ &\quad + J_m n^2)(-M_2R_wL\psi - 2M_3LR_w\psi)\dot{\psi} + (-M_2R_w^2 \\ &\quad -M_3R_w^2 - J_w - M_2R_wL - 2M_3LR_w - 2J_m n^2)\beta / D_{pit} , \\ A_{24} &= -(-M_2R_w^2 - M_3R_w^2 - J_w - M_2LR_w - 2M_3LR_w \\ &\quad -2J_m n^2)\beta / D_{pit} , \\ A_{41} &= -(M_2LR_w + 2M_3LR_w + + J_m n^2)(M_2 + 2M_3)gL / D_{pit} , \\ A_{42} &= -(M_2LR_w + 2M_3LR_w + J_m n^2)(-M_2L^2\psi - 4M_3L^2\psi)\dot{\psi} \\ &\quad +(M_2L^2 + M_3 4L^2 - J_m n^2 + J_\psi)(-M_2LR_w\psi + M_2L^2 \\ &\quad -2M_3LR_w\psi)\dot{\psi} - (M_2LR_w + 2M_3LR_w \end{aligned}$$

This article has been accepted for publication in a future issue of this journal, but has not been fully edited. Content may change prior to final publication. Citation information: DOI 10.1109/TIE.2014.2327562, IEEE Transactions on Industrial Electronics

$$+4M_3L^2 + J_\psi)\beta / D_{pit},$$

$$A_{44} = (M_2LR_w + 2M_3LR_w + M_2L^2 + 4M_3L^2 + J_\psi)\beta / D_{pit},$$

$$B_{21} = (-M_2R_w^2 - M_3R_w^2 - J_w - M_2LR_w - 2M_3LR_w - 2J_m n^2)\alpha / D_{pit},$$

$$B_{41} = (M_2LR_w + 2M_3LR_w + M_2L^2 + 4M_3L^2 + J_\psi)\alpha / D_{pit},$$

and

$$D_{pit} = (M_2R_w^2 + M_3R_w^2 + J_w + J_m n^2)(M_2L^2 + M_3 4L^2 - J_m n^2 + J_\psi) - (M_2LR_w + 2M_3LR_w + J_m n^2)^2.$$

The desired set point is given as

$$x = x_d. \tag{20}$$

Then $\exists u_d$ is chosen such that

$$\dot{x}_d = Ax_d + Bu_d. \tag{21}$$

We can define the error variables, $\tilde{u} = u_p - u_d$ and $\tilde{x} = x - x_d$, which satisfy $\dot{\tilde{x}} = A\tilde{x} + B\tilde{u}$.

LQR control is one of the optimal control methods, and it requires finding an optimal state feedback gain that minimizes the performance index. The performance index is defined as follows [22], [23]:

$$J = \int_0^\infty [\tilde{x}(t)^T Q\tilde{x}(t) + \tilde{u}(t)^T R\tilde{u}(t)]dt, \tag{22}$$

where Q and R are weight matrices that are key factors in determining the performance of the optimal control.

State feedback control inputs are expressed as follows:

$$\tilde{u}(t) = -K\tilde{x}(t), \tag{23}$$

where the state feedback gains are obtained as $K = R^{-1}B^T P$, and P will be determined uniquely as a solution of the Riccati equation as follows:

$$A^T P + PA - PBR^{-1}B^T P + Q = 0. \tag{24}$$

From this Riccati equation, the P matrix is uniquely determined, and it is used to calculate the state feedback gain K .Thus, the control input can be obtained from (24) as follows:

$$u_p = -K\tilde{x} + u_d, \tag{25}$$

where u_d contains the command input. Now, for the optimal LQR control, the matrices R and Q are required to be defined for application to the Riccati equation. R is selected as an identity matrix, and Q is selected through several trial and error experiments as follows:

$$Q = \begin{bmatrix} 150 & 0 & 0 & 0 \\ 0 & 5 & 0 & 0 \\ 0 & 0 & 5 & 0 \\ 0 & 0 & 0 & 25 \end{bmatrix}. \tag{26}$$

For the given A, B, R, and Q matrices, the optimal state feedback control is determined by solving the Riccati equation as follows:

$$K = \begin{bmatrix} -124.1 & -37.8 & -2.2 & -6.6 \end{bmatrix}. \tag{27}$$

B. Roll controller

The sliding mode control is known as a robust algorithm, which can properly control nonlinear and uncertain systems characterized by parameter variations, disturbances, and modeling errors. For roll control, the robust sliding mode controller is adopted in this study. The nonlinear roll dynamic model for the unicycle robot is given as

$$\ddot{\theta}_R = f(\theta_R, \dot{\theta}_R) + g_{roll}u_{roll} + F_u. \tag{28}$$

where $g_{roll} = -2\alpha J_d / D_{roll}$, $D_{roll} = [(M_1R_w^2 + M_2(R_w^2 + L^2 + 2LR_w) + M_3(R_w^2 + 4L^2 + 4LR_w) + J_d)J_d - J_d^2]$, u_{roll} and $f(\theta_R, \dot{\theta}_R)$ are given in (29) and (33), respectively, and F_u denote the uncertainties of the system including modeling error and external disturbance given in (33). Notice that F_u can be compensated by u_s which is called a robust control input.

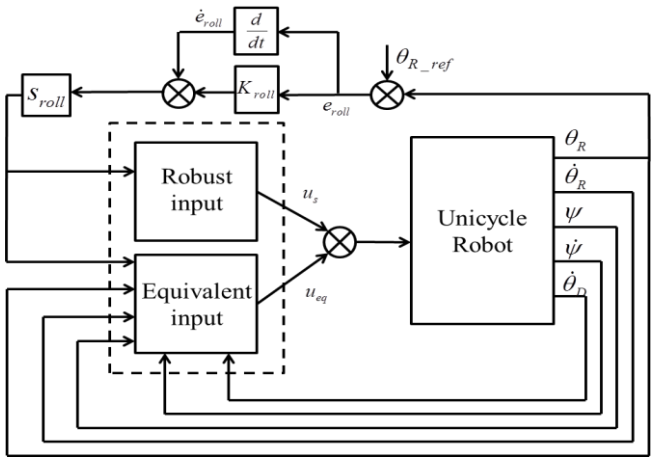

Fig. 5. Block diagram of the sliding mode control of the roll controller.

The control input of the sliding mode control can be represented as the sum of the equivalent and robust inputs:

$$u_{roll} = u_{eq} + u_s, \tag{29}$$

where u_{eq} and u_s are defined in (34) and (35). The foregoing design process is applied to design the sliding mode control of the roll axis of the unicycle robot. Figure 5 shows the block diagram of a sliding mode controller designed for the roll axis. The sliding surface of the roll control is defined as [17-19]

This article has been accepted for publication in a future issue of this journal, but has not been fully edited. Content may change prior to final publication. Citation information: DOI 10.1109/TIE.2014.2327562, IEEE Transactions on Industrial Electronics

$$s_{roll} = K_{roll} e_{roll} + \dot{e}_{roll}, \tag{30}$$

where $K_{roll} > 0$ is a design constant and e_{roll} is the difference between the reference input and the current roll angle, which is defined as

$$e_{roll} = \theta_R - \theta_{R\_ref}. \tag{31}$$

The time derivative of s_{roll} is used to find the equivalent input, u_{eq}, as follows:

$$\begin{aligned} \dot{s}_{roll} &= K_{roll}\dot{e}_{roll} + \ddot{e}_{roll} \\ &= K_{roll}\dot{e}_{roll} + \ddot{\theta}_R - \ddot{\theta}_{R\_ref}, \end{aligned} \tag{32}$$

where $\ddot{e}_{roll} = \ddot{\theta}_R - \ddot{\theta}_{R\_ref}$, and $\ddot{\theta}_R$ can be obtained from the dynamic equations expressed in terms of voltage inputs. The simplified dynamics of $\ddot{\theta}_R$ is obtained from (13) and (15) as follows:

$$\begin{aligned} \ddot{\theta}_R =& \Big[-J_d M_2(-L^2\theta_R - 2LR_w\theta_R)\dot{\theta}_R - J_d(M_2L^2\psi + M_3(-4L^2\psi \\ & -2LR_w\psi))\dot{\psi} - J_d(M_1gR_w\theta_R + M_2g(R_w\theta_R + L\theta_R) \\ & + M_3g(R_w\theta_R + 2L\theta_R)) - 2\alpha J_d V \\ & + 2J_d\beta(\dot{\theta}_D - \dot{\theta}_R)\Big] / D_{roll} \\ =& \bar{f}(\theta_R, \dot{\theta}_R) - \bar{g}_{roll} u_{roll} + F_u, \end{aligned} \tag{33}$$

where $f(\theta_R, \dot{\theta}_R) = \Big[-J_d M_2(-L^2\theta_R - 2LR_w\theta_R)\dot{\theta}_R - J_d(M_1gR_w\theta_R + M_2g(R_w\theta_R + L\theta_R) + M_3g(R_w\theta_R + 2L\theta_R)) - 2J_d\beta\dot{\theta}_R \Big] / D_{roll}$, $\bar{f}(\theta_R, \dot{\theta}_R)$ is a nominal value of $f(\theta_R, \dot{\theta}_R)$, $\bar{g}_{roll}$ denotes the nominal value of g_{roll}, $F_u = [-J_d(M_2L^2\psi + M_3(-4L^2\psi + F_d - 2LR_w\psi)\dot{\psi} + 2J_d\beta\dot{\theta}_D + \Delta f] / D_{roll}$, F_d is an external disturbance, and Δf is a modeling error. Letting $\dot{s} = 0$, the control input, which is called an equivalent input, u_{eq}, makes both e_{roll} and $\dot{e}_{roll}$ to be null. u_{eq} is derived as follows:

$$u_{eq} = -\frac{1}{\bar{g}_{roll}} \Big[K_{roll}\dot{e}_{roll} - \ddot{\theta}_{R\_ref} + \bar{f}(\theta_R, \dot{\theta}_R) \Big], \tag{34}$$

$$u_s = -\gamma_{roll} sgn(s_{roll}) / \bar{g}_{roll}, \tag{35}$$

where γ_{roll} is a strictly positive design constant, and sgn is the signum function. The Lyapunov function is defined as follows:

$$V = \frac{1}{2} s_{roll}^2. \tag{36}$$

The time derivative of (36) using (32), (33), (34), and (35) can be given as follows:

$$\dot{V} = s_{roll}\dot{s}_{roll} = -\gamma_{roll} |s_{roll}| \le 0. \tag{37}$$

Therefore, $\dot{V}$ is negative for all $s_{roll} \neq 0$. This means that $s_{roll} \to 0$ as $t \to \infty$. The reaching condition is then satisfied [17] and the steady state tracking performance can be guaranteed by (30) with a positive parameter K_{roll}. Therefore, it is proved that $e_{roll} \to 0$ as $t \to \infty$. However, the control law of (35) is discontinuous across $s_{roll}(t)$. This leads to chattering in the control input and may excite a high frequency system dynamics. Thus, a sigmoid function, $\tanh(s_{roll})$, is employed as the switching function to reduce the chattering phenomenon [25].The roll control input is the sum of the equivalent input and a robust control input, which is sum to make the system stable. (35) is replaced the following control:

$$u_s = -\gamma_{roll} \tanh(s_{roll}). \tag{38}$$

Therefore, for the roll attitude tracking of unicycle robot, a desired control performance can obtained without excessive chattering using the sliding mode controller.

IV. EXPERIMENTS

A. Descriptions of the experimental equipment

The IMU sensor is placed on the center of the body to simultaneously get the pitch and roll angles of the robot. At the center of the body, the coordinates of the roll and pitch axes are defined. The sensory data are transmitted to the main MCU (LM3S8962) through RS-232 communication channel in every 10 msec. For the roll and pitch control, MAXON DC motors are utilized to rotate the disc of the top and the wheels of the bottom. The DC motors are driven by NT-DC20A H-bridge type drive. The motor torque and rotation speed are controlled by the PWM signal from the drive.

B. Switching function

It is known that the sliding mode controller with a signum switching function causes chattering in the control input. Therefore, to reduce chattering, a hyperbolic tangent function, which is a kind of sigmoid function, is used in this study as a switching function in (38). The effect of chattering reduction by the sigmoid function is illustrated in Fig. 6. When the signum function is used as the switching function, the system finally becomes unstable because a high frequency robot dynamics is excited owing to chattering.

The control performance of the single-wheel robot has been checked for a straight line motion with a step velocity command and the desired velocity profile. For each experiment, the roll and pitch angles are measured and displayed to show the stability of the unicycle robot during driving.

C. Step velocity

In Fig. 7, the solid line represents the distance of the mobile robot from the origin for the given step velocity input, and the broken line represents the real distance for 30 *s* of driving. Figure 8 illustrates the

This article has been accepted for publication in a future issue of this journal, but has not been fully edited. Content may change prior to final publication. Citation information: DOI 10.1109/TIE.2014.2327562, IEEE Transactions on Industrial Electronics

desired and actual velocities of the unicycle robot with the proposed control algorithm for 0.08 *m/s* step command input. The velocity-tracking performance could not be very good because the unicycle robot should maintain its balance while trying to follow the desired velocity trajectory. However, comparing the result of Fig. 8 with that of [26], it has been observed that the frequency of the velocity-tracking error is lower and the magnitude is smaller with the proposed algorithm than with the previous one using the decoupled dynamic model.

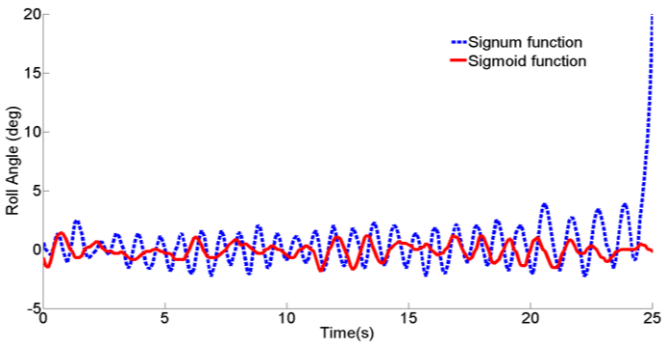

Fig. 6. Balancing control data with sigmoid and signum functions.

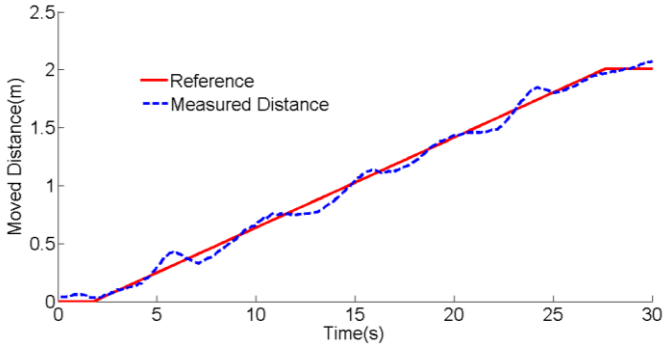

Fig. 7. Measured distance data with straight line driving.

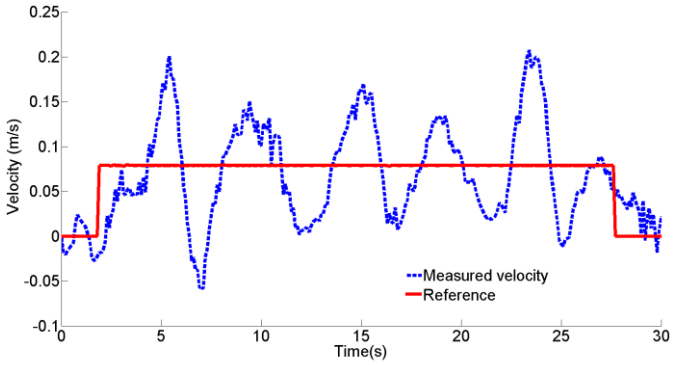

Fig. 8. Measured velocity data with straight line driving.

Figure 10 represents the changes of the roll angle during the straight line motion. The roll angle is kept within $\pm 2^{\circ}$, which is one of the main reasons for the velocity-tracking error. Figure 11 illustrates the pitch angle error while the unicycle robot is driving to the goal. The errors are kept within $\pm 2.5^{\circ}$. The pitch control error is coupled to the roll control effort. That is, while the unicycle robot is maintaining its balance, it is not capable of controlling its driving speed precisely. Notice that the pitch angle has a small positive value for forward driving. A slightly forward tilted posture is effective for the forward motion if the tilt angle can be controlled precisely.

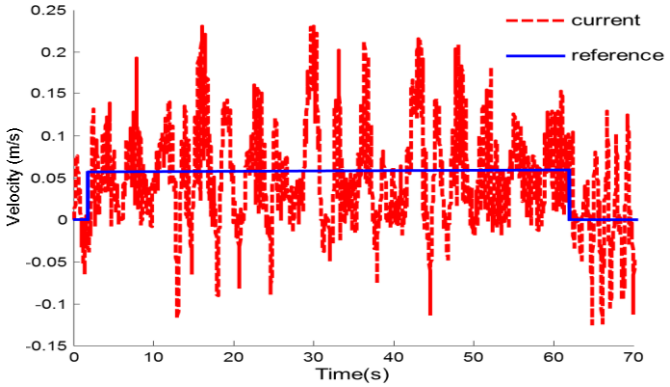

Fig. 9. Velocity data for the step input using the decoupled dynamic model.

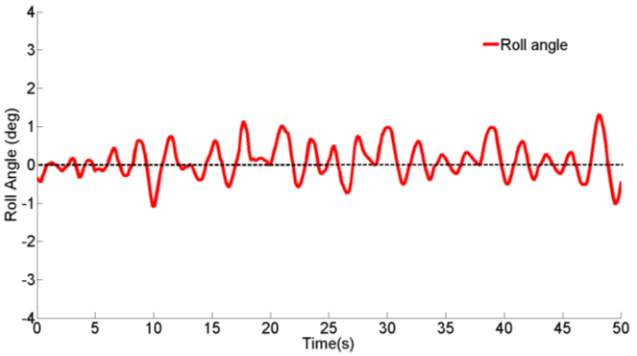

Fig. 10. Measured roll angle data with straight line driving.

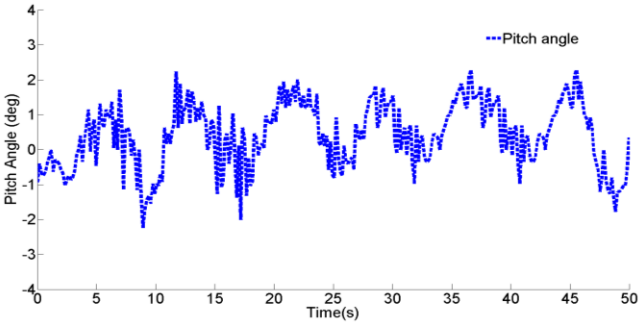

Fig. 11. Measured pitch angle data with straight line driving.

D. Trapezoidal velocity profile

To generalize the velocity control, it is planned to impose the trapezoidal velocity profile on the unicycle robot (Fig. 12 solid line). The first and last 5*s* in Fig. 12 are used for stabilizing the unicycle robot. From 5*s* to 25*s*, the velocity is increased linearly, whereas from 45*s* to 65*s*, the velocity is decreased linearly. Between 25*s* and 45*s*, the velocity is planned to be constant.

Figure 12 illustrates the velocity-tracking performance of the proposed algorithm. The solid line is for the reference velocity, and the dashed line is for the actual velocity. Note that the velocity -tracking performance is greatly improved compared with Fig. 13, which is obtained by decoupling the controls of the roll and pitch axes

This article has been accepted for publication in a future issue of this journal, but has not been fully edited. Content may change prior to final publication. Citation information: DOI 10.1109/TIE.2014.2327562, IEEE Transactions on Industrial Electronics

[26]. The improvement in the velocity-tracking performance is very similar to that of the step velocity input. Figure 14 illustrates the planned and actual distances of the unicycle robot from the origin. The actual distance slightly deviated from the planned distance with time.

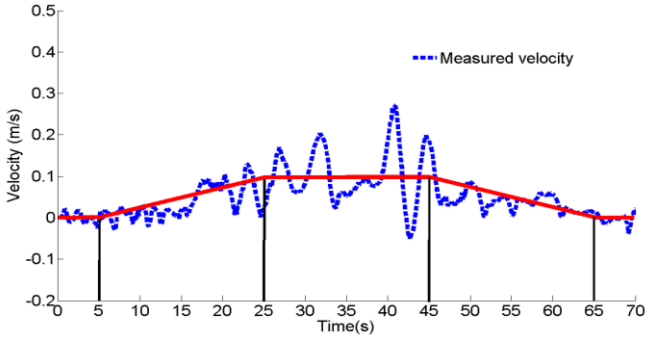

Fig. 12 . Measured velocity data with speed-controlled driving.

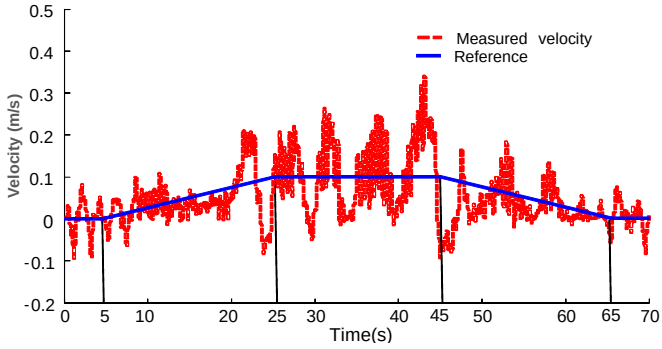

Fig. 13. Velocity data using the decoupled dynamic model .

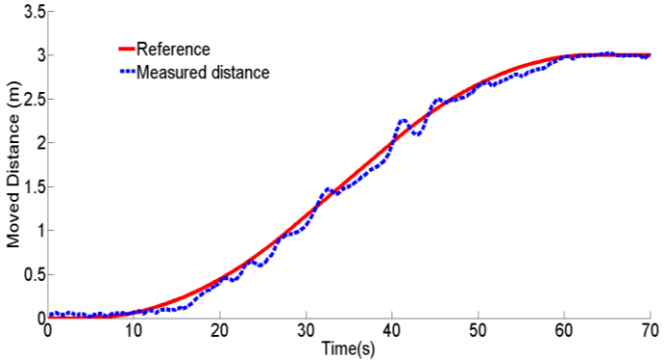

Fig. 14. Measured distance data with speed-controlled driving.

Figure 15 illustrates that the roll axis error is maintained within $\pm 1.5^{\circ}$ stably while the unicycle robot is driving with the desired velocity profile. Even though the velocity is increased, the roll angles are kept within a very stable range. Figure 16 shows that the pitch angle is kept within $\pm 3^{\circ}$ with speed -controlled driving. The pitch vibration angle is bigger than the roll angle error since pitch control is required for driving while maintaining a stable posture.

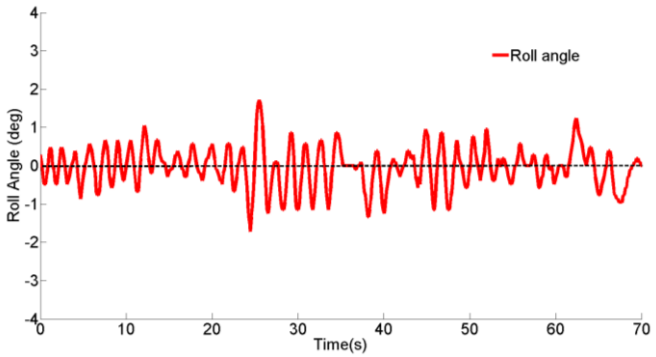

Fig. 15. Measured roll angle data with speed-controlled driving.

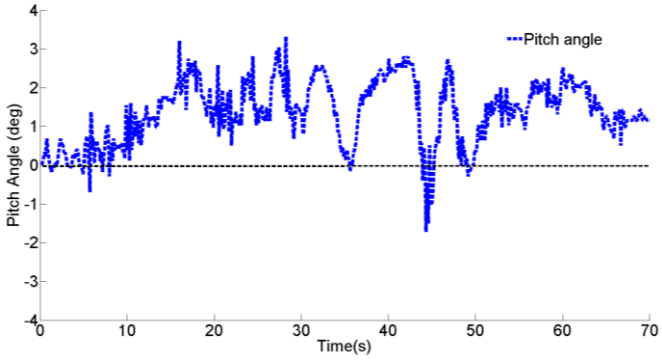

Fig. 16. Measured pitch angle data with speed-controlled driving.

V. Conclusion

This paper proposes a unified control system for the unicycle robot based on the derived dynamic model. For the control of left-right balance, roll-axis control is implemented using the sliding mode control algorithm, and velocity tracking control is achieved by pitch control using the LQR controller with stable posture control. It is verified that the derived dynamic model includes complex coupling terms between the roll and pitch axes, which implies that the unified control system provides better velocity control performance than the previously proposed decoupled control algorithm. For roll control, the sliding mode controller is adopted, and the switching function employs the hyperbolic tangent function instead of the signum function to reduce chattering. With the step input velocity and the trapezoidal velocity commands, the velocity-tracking performance of the proposed algorithm has been verified. With unified, concurrent control of the roll and pitch axes, the velocity-tracking performance has greatly improved compared with that of the conventional decoupled control algorithm. Even though the sigmoid function is utilized for the sliding mode control of roll axis, still there was small chattering in the output. To minimize this chattering, a sliding mode observer can be adopted as a future research work.

References

[1] I. Fantoni, R.Lozano and M. Spong "Energy based control of the Pendubot, " *IEEE Trans. A. C.*, vol. 45, no. 4, pp. 725-729, April, 2000.

[2] J. Constantin, C. Nasr and D. Hamad, "Control of robot manipulator and pendubot system using artificial neural networks, " *Robotica*, vol. 23, no. 6, pp. 781-784, 2005.

[3] C. C. Tsai, C. K. Chan, S. C. Shih, and S. C. Lin, "Adaptive nonlinear control using RBFNN for an electric unicycle," *IEEE International conference on systems Man and Cyber., SMC 2008*, pp. 2343-2348, (2008).

[4] A. Schoonwinkel, "Design and test of a computer stabilized unicycle," Ph. D. dissertation, Stanford Univ., 1987.

[5] Z. Sheng and K. Yamafuji, "Postural stability of a human riding a unicycle and its emulation by a robot," *IEEE Trans. Robotics and Autom.*, vol. 13, no. 5, pp. 709 - 720, Oct. 1997.

[6] J. O. Lee, S. I. Han, I. W. Han, S. I. Lee, and J. M. Lee "Attitude and direction control of the unicycle robot using fuzzy-sliding mode control," *Journal of Institute of Control, Robotics and Sys.*, vol. 18, no. 3, pp. 275 - 284, Mar. 2010.

[7] H. Jin, J. Hwang, and J. M. Lee "A balancing control strategy for a one-wheel pendulum robot based on dynamic model decomposition: simulations and experiments," *IEEE/ASME Trans. Mechatronics*, vol. 16, no. 4, pp. 763 – 768, Aug. 2011.

[8] S.. H. Kim, J. O. Lee, J. Hwang, B. Ahn, and J. M. Lee, "Dynamic modeling and performance improvement of a unicycle robot," *Journal of Institute of Control, Robotics and Sys.*, vol. 16, no. 11, pp. 1174 - 1181, Nov. 2010.

[9] H. Lim, J. Hwang, B. Ahn, and J. M. Lee, "Robust yaw motion control of unicycle robot," *Journal of Institute of Control, Robotics and Sys.*, vol. 15, no. 11, pp. 1130 - 1136, Nov. 2009.

[10] http://www.muratagirl.com.

[11] H. Ohsaki, M. Iwase, T. Sadahiro, and S. Hatakeyama, "A consideration of human-unicycle model for unicycle operation analysis based on moment balancing point," *Proc. of the 2009 IEEE Int. Conf. Systems, Man, and Cyber.*, pp. 2468 -2473, Oct., 2009.

[12] S. C. Lin, C. C. Tsai, X. Q. Shih, and C. H. Lu, "Linearized two-loop posture and speed control of an electric unicycle," *Proc. of the 2010 Int. Conf. System Science and Eng.*, pp. 245 -250, 2010.

[13] A. Kadis, D. Caldecott, A. Edwards, and M. Jerbic, "Modelling, simulation and control of an electric unicycle," *Proc. of the 2010 Australasian Conf. Robotics & Autom.*, pp.1-8, Dec., 2010.

[14] S. Zhiyu, and L. Daliang, "Balancing control of a unicycle riding," *Proc. of the 29th Chinese Control Conf.*, pp. 3250 -3254, 2010.

[15] J. H. Lee, H. J. Shin, S. J. Lee, and S. Jung, "Novel air blowing control for balancing a unicycle robot," *Proc. of the 2010 IEEE/RSJ Inter. Confer. Intelligent Robotics and Sys.*, pp. 2569 -2530, 2010.

[16] X. Ruan, X. Zhu, Y. Li, and R. Wei, "Lateral stabilization of a single wheel robot applying electromagnetic force," *Proc. of the 10th World Congress Intelligent Control and Autom.*, pp. 3675-3680 , 2012.

[17] J. E. Slotine and W. Li, *Applied nonlinear control*, Englewood Cliffs: New Jersey, 1991.

[18] R. de Castro, R. E. Araujo and D. Freitas, "Wheel slip control of EVs based on sliding mode technique with conditional integrators," *IEEE Trans. Ind. Electron.*, vol. 60, no. 8, pp. 3256-3271, June, 2013.

[19] C. Evangelista, P. Puleston, F. Valenciaga, and L. M. Fridman, "Lyapunov-designed super-twisting sliding mode control for wind energy conversion optimization," *IEEE Trans. Ind. Electron.*, vol. 60, no. 2, pp. 538 -545, Feb. 2013.

[20] H. Li, J. Yu, C. Hilton, and H. Liu, "Adaptive sliding-mode control for nonlinear active suspension vehicle systems using T–S fuzzy approach," *IEEE Trans. Ind. Electron.*, vol. 60, no. 8, pp. 3328 - 3338, Aug., 2013.

[21] D. Ginoya, P. D. Shendge, and S. B. Phadke, "Sliding mode control for mismatched uncertain systems using an extended disturbance observer," *IEEE Trans. Ind. Electron.*, vol. 61, no. 4, pp. 1983 -1992, April, 2014.

[22] D. Bernstein, and W. Haddad, "Optimal output feedback for nonzero set points regulation," *IEEE Trans. A. C.*, vol. 32, no. 7, pp. 642 -645, July, 1987.

[23] W. Haddad, and D. Bernstein, "Optimal output feedback for non-zero set point regulation: the discrete-time case," *Int. J. of Control*, vol. 47, no. 2, pp. 529-536, 1988.

[24] X. Ruan, Q. Wang , and N. Yu, "Dual-loop adaptive decoupling control for single wheeled robot based on neural PID controller," *2011 11th Int. Conf. Control, Automation, Robotics and Vision*, pp. 2349 - 2354, Dec. 2010.

[25] J. B. Son, H. R. Kim, Y. S. Seo, and J. M. Lee, "PMSM sensorless speed control using a high speed siding mode observer," *Journal of Institute of Control, Robotics and Sys.*, vol. 16, no. 3, Mar. 2010.

[26] J. O. Lee, S. I. Han, and J. M. Lee, "Decoupled dynamic control for pitch and roll axes of the unicycle robot," *IEEE Trans. Ind. Electron.*, vol. 60, no. 9, pp. 3814 -3822, Sept., 2013.

Seong I. Han (M'12) received the B.S. and M.S. degrees in mechanical engineering from Pusan National University, Busan, Korea, in 1987 and 1989, respectively, and the Ph. D. in mechanical design engineering from Pusan National University, Busan, in 1995. From 1995 to 2009, he was an associate professor of electrical automation of Suncheon First College, Korea. Now he is with the Department of electronic engineering, Pusan National University, Korea. His research interests include intelligent control, nonlinear control, robotic control, vehicle system control, and steel process control.

Jang M. Lee (SM'03) received the B.S. and M.S. degree in electronic engineering from Seoul National University, Seoul, Korea, in 1980 and 1982, respectively, and the Ph. D. degree in computer engineering from the University of Southern California, Los Angeles, in 1990.

Since 1992, he has been a Professor with Pusan National University, Busan, Korea. He was the Leader of the "Brain Korea 21 Project" of Pusan National University. His research interests include intelligent robotics, advanced control algorithm, and specialized environment navigation/localization. Prof. Lee was the former president of the Korean Robotics Society.